Magn Reson Mater Phy (2013) 26:127–136
DOI 10.1007/s10334-012-0339-2

RESEARCH ARTICLE

Evaluation of an attenuation correction method for PET/MR imaging of the head based on substitute CT images

Anne Larsson · Adam Johansson · Jan Axelsson · Tufve Nyholm · Thomas Asklund · Katrine Riklund · Mikael Karlsson

Received: 2 April 2012 / Revised: 15 August 2012 / Accepted: 20 August 2012 / Published online: 7 September 2012

Abstract
Object The aim of this study was to evaluate MR-based attenuation correction of PET emission data of the head, based on a previously described technique that calculates substitute CT (sCT) images from a set of MR images.
Materials and methods Images from eight patients, examined with ^{18}F-FLT PET/CT and MRI, were included. sCT images were calculated and co-registered to the corresponding CT images, and transferred to the PET/CT scanner for reconstruction. The new reconstructions were then compared with the originals. The effect of replacing bone with soft tissue in the sCT-images was also evaluated.
Results The average relative difference between the sCT-corrected PET images and the CT-corrected PET images was 1.6 % for the head and 1.9 % for the brain. The average standard deviations of the relative differences within the head were relatively high, at 13.2 %, primarily because of large differences in the nasal septa region. For the brain, the average standard deviation was lower, 4.1 %. The global average difference in the head when replacing bone with soft tissue was 11 %.
Conclusion The method presented here has a high rate of accuracy, but high-precision quantitative imaging of the nasal septa region is not possible at the moment.

Keywords PET/MR · Attenuation correction · Substitute CT · ^{18}F-FLT · UTE

A. Larsson (✉) · A. Johansson · J. Axelsson · T. Nyholm · T. Asklund · K. Riklund · M. Karlsson
Department of Radiation Sciences, Umeå University, 90187 Umeå, Sweden
e-mail: anne.larsson.stromvall@vll.se

Introduction

Interest in combining positron emission tomography (PET) and magnetic resonance imaging (MRI) has grown considerably in recent years [1]. A number of integrated small-animal PET/MR systems are in use for research purposes, and an increasing number of commercial whole-body systems are available for patient imaging [2]. PET is usually combined with computed tomography (CT), but PET/MR is expected to become an increasingly important clinical and research tool in the future, due to the superior soft tissue contrast of MRI. A PET/MR scanner can also provide functional MR imaging such as MR-diffusion and MR spectroscopy.

The problem of how to correct for attenuation of the PET annihilation photons has not been fully solved in PET/MR. CT images acquired during PET/CT can be recalculated to attenuation maps in a straightforward manner because of the clear correlation of CT with tissue electron density [3], but this is not possible in PET/MR. Many different techniques have been proposed for the conversion of MR images to attenuation maps [4–7]. Several methods are based on either segmentation of tissues or atlas-based approaches [8–13] and reliable results have been presented. Atlas-based approaches, however, will give less certain results in cases of abnormal anatomy. A problem for many methods is that compact bone normally does not give any measurable MR signal because of short T2 relaxation times, and it has therefore been difficult to separate bone from air when calculating the attenuation maps. Using sequences with ultra-short echo times (UTE) [14] has been proposed [5], since such sequences can sample signals from cortical bone, making the differentiation possible.

The aim of the work presented here was to evaluate a method for attenuation correction of PET images of the

head, based on voxel-based substitute CT (sCT) images derived from a set of UTE and T2-weighted MR sequences. This method has been described in a previous publication from our group [15]. In short, this method is based on a Gaussian mixture regression (GMR) model, which links the MR voxel values to Hounsfield units (HU). The technique can generate CT-like images with a mean absolute error of 137 HU and showed the largest uncertainties at interfaces between air and tissue and between bone and tissue. However, the accuracy was much higher within the brain [16]. The method has been applied to imaging of the head. No assumptions about patient anatomy are made and it should therefore be possible to use the method in cases including anatomic abnormalities. More specifically, the aim was to evaluate the errors introduced when the original CT images are replaced by the sCT images for the purpose of attenuation correction of the PET emission data. The method was analysed in a clinical setting with glioma patients, imaged with both PET/CT and MR. Another aim was to evaluate the importance of including bone, and not just soft tissue, in the sCT attenuation maps.

Materials and methods

Patients

For a realistic evaluation of the errors introduced in the head region when replacing CT with sCT, this study was included in an ongoing project called "Evaluation of ^{18}F-FLT PET and advanced MR techniques for development of early biomarkers for the treatment effects of malignant brain tumours" at Umeå University. The study is approved by the ethical and radiation safety committees at Umeå University Hospital, Sweden. In this project, nine patients diagnosed with high-grade malignant glioma have so far been included after being given oral information about the study and after giving their informed consent. All patients were treated with conformal radiotherapy consisting of 2 Gy fractions daily to a total dose of 60 Gy concomitant with administration of temozolomide, followed by adjuvant temozolomide [17]. The patients were imaged with ^{18}F-3′-fluoro-3′-deoxy-L-thymidine (^{18}F-FLT) PET and MRI at baseline and 2 weeks after the start of treatment. ^{18}F-FLT is a tracer substance that can be used to image tumour proliferation [18], and it has a better predictive power for tumour progression and survival of malignant glioma than ^{18}F-fluorodeoxyglucose (^{18}F-FDG) [19]. The PET and MRI scans were performed 1–3 days apart. One of the nine patients was excluded from the study because of incomplete image data.

PET/CT imaging

The PET/CT images were acquired on a Discovery 690 PET/CT scanner (General Electric, WI, US) at the Nuclear Medicine Department, Umeå University Hospital. The scanner is equipped with 24 rings of lutetium-yttrium-orthosilicate (LYSO) PET detectors, and acquires images in 3D. The axial length of the field of view (FOV) is 15 cm. The CT included in the system is a 64-slice scanner. The patients were given an intravenous injection of ^{18}F-FLT, 2.6 MBq/kg body weight, and were lightly fixated with wedge-shaped cushions in the head holder and with a Velcro tape over the forehead.

We initially intended to carry out a one-FOV 1.5 h dynamic ^{18}F-FLT study of the brain, and two dynamic scans were accordingly obtained from the first patient. A dynamic study of this length was, however, too tiresome for these patients, and the rest of the PET scans were acquired as static scans over the head and neck region. These scans included three consecutive bed positions with an acquisition time of 4 min each. The clinical protocol also included a body scan, which is not described here. The PET/CT examination started 90 min after injection, and the patient rested during the period between injection and scanning.

The CT images were acquired using the standard brain protocol at Umeå University Hospital: 120 kVp, Auto-mA and Smart-mA (noise index = 10), with a slice thickness of 0.625 mm. For PET attenuation correction, a reconstruction devoted to this purpose, "AC for PET" was performed with a down-sampled slice thickness of 3.75 mm. The CT images were reconstructed in 512 × 512 matrices to a FOV of 70 cm.

The PET images were reconstructed to a FOV of 25 cm in 256 × 256 pixel matrices with a slice thickness of 3.27 mm. The dynamic series obtained from patient 1 consisted of 47 slice images, while the three-FOV head and neck protocol used for the rest of the patients resulted in 119 images per patient. The reconstruction method was VUE-point HD (General Electric, WI, US), which is a fully 3D iterative algorithm based on ordered subsets expectation maximisation (OSEM), using a resolution recovery method, "SharpIR". VUE-point HD includes normalisation, compensation for dead-time, a model for detector geometry, and correction for attenuation and scatter. The number of OSEM iterations was set to 6 (24 subsets) and a Gaussian post-filter with 3.0 mm full width at half maximum (FWHM) was used.

All images, including the PET raw data, were saved in a local digital research archive, DCM4CHEE (http://www.dcm4che.org/), at the Nuclear Medicine Department.

MR imaging

The sCT method [15] was developed on a 1.5 T MR-scanner. The MR images in the current study were therefore also acquired on a 1.5 T scanner, a Siemens Espree (Siemens AG, Erlangen, Germany) at the Radiation Therapy Department, Umeå University Hospital. The scanner is equipped with a four-segment head coil, in which the patients were lightly fixated with cushions. Several MR sequences were recorded with a total scanning time of about 60 min in order to evaluate early treatment response. Only two dual-echo UTE sequences with different flip angles and a 3D T2-weighted sequence (SPACE) have been considered during the work described here [15].

The two dual-echo UTE sequences sampled the free induction decay (FID) with an echo time of 0.07 ms and a second gradient echo after 3.76 ms, both from the same excitation. The first UTE sequence had a flip angle of 10° and the flip angle for the other UTE sequence was set to 60°. These parameters were chosen to enable us to distinguish between tissues with short and long T2*, and to distinguish between tissues with the same short T2* which differed in T1. TR was 6 ms for both sequences, and the images were reconstructed in 192 × 192 × 192 pixel matrices with an isotropic voxel size of 1.33 mm. The acquisition time was 3 min for each dual-echo UTE sequence, and each sequence resulted in two separate images, one for each echo time.

A T2-weighted 3D SPACE scan was also recorded to distinguish between tissues with a long T1 and air. SPACE is a Siemens 3D turbo spin echo sequence with variable flip angle refocusing pulses. The parameters for this scan were: TE: 100 ms, TR: 1,500 ms, flip angle: 150° and a voxel size of 0.78 × 0.78 × 1.7 mm. The acquisition time was 5 min.

The MR images were corrected for spatial distortion by a standard algorithm provided by Siemens [20], and a low resolution pre-scan was used to correct for inhomogeneous coil sensitivity.

The total scanning time of the three sequences was 11 min. For the sake of patient comfort, these sequences were only included during the baseline scanning before the start of treatment, since no major structural differences were expected to occur during the 2-week period between baseline and follow-up.

Attenuation correction

The five sets of MR images from each patient (four UTE image sets and one SPACE set) were recalculated into a set of sCT images using a GMR model that linked the intensities in the MR images to Hounsfield units. This method has been described in a previous article that presents the sCT method [15]. Two additional images were derived from each MR image during this process by calculating the average value and standard deviation in a 27-voxel neighbourhood around each MR voxel. The original MR images and their filtered siblings formed an expanded set of MR images. The GMR model assumes that the joint distribution of intensities of the voxels in the expanded MR image set and the corresponding Hounsfield values can be modelled by a Gaussian mixture model (GMM) distribution according to:

$$f_{\mathbf{Z}}^{\text{mix}}(\mathbf{z}) = \sum_{i=1}^{N} a_i \frac{1}{(2\pi)^{k/2}|\Sigma_i|^{1/2}} \exp\left(-\frac{1}{2}(\mathbf{z}-\boldsymbol{\mu}_i)^T \Sigma_i^{-1}(\mathbf{z}-\boldsymbol{\mu}_i)\right) \quad (1)$$

where $\mathbf{z}$ is the vector of expanded MR intensities and Hounsfield values and a_i, $\boldsymbol{\mu}_i$ and $\sum_i$ are parameters describing the distribution. N is the number of multivariate Gaussians used (20) and k is the vector length of $\mathbf{z}$ which is 16 (15 MR sets and 1 CT set) [15]. The maximum likelihood estimates of these parameters can be obtained using expectation maximization (EM). The estimation used a dataset of co-registered MR and CT images. The sCT images in the present study were calculated using the pre-estimated parameter values for the GMR model. The Hounsfield value of each voxel is given by the conditional expectation of the GMM distribution, given the observed expanded MR intensities in that voxel [15]. The conditional expectation was calculated using software implemented using Matlab (The Mathworks, Inc., MA, US).

The calculated sCT images were then co-registered to the patient's "AC for PET" image series using the rigid co-registration tool in the SPM8 software (Wellcome Department of Imaging Neuroscience, London, UK), implemented in Matlab. The sCT images were also smoothed in SPM8 using a 3D symmetrical 3 mm FWHM Gaussian filter kernel to obtain the same resolution as a typical attenuation map. The outcome of co-registration was evaluated by visual inspection. SPM8 operations were performed using the NIfTI image format, and conversion from the standard DICOM format to NIfTI was performed using the dcm2nii software included in the MRIcron package: (http://www.mccauslandcenter.sc.edu/mricro/mricron/index.html).

The PET/CT head holder was clearly visible in the CT images, whereas the sCT images were without a visible head holder. We copied, therefore, the CT head holder from the CT images to the sCT images after co-registration in order to enable a fair comparison between the CT-based and the sCT-based attenuation corrections. This was performed in Matlab using a manually defined region of interest (ROI) around the contours of the CT head holder in a central slice. Some of the low-density patient positioning aids were also included in this ROI. The ROI was applied

to all CT images of the head, and the contents of the ROIs were then copied to the corresponding sCT images. The ROI was thick enough to allow for a few degrees of possible tilting of the head holder, and the result for each study was evaluated by visual inspection. A sagittal CT image and the corresponding co-registered sCT image, with the added head holder, are presented in Fig. 1 (patient 6, scan 1).

This study also aimed to determine the importance of including bone in the sCT method, for the purpose of attenuation correction. Bone-free sCT images were therefore calculated by setting all HU values greater than 40 to 40. ICRP 89 [21] states that the specific gravity of brain tissue is 1.04, and an HU value of 40 should therefore be a representative value for brain tissue, assuming a linear relationship between density and HU, between air and soft tissue.

The co-registered sCT images, in NIfTI format, required reconversion to the DICOM format before being transferred to the PET/CT scanner. In-house software, imlook4d (http://code.google.com/p/imlook4d), was used for this purpose, and the sCT images were saved as a new "AC for PET" series. A reconstruction was then performed on the PET/CT scanner with the new set of sCT data as input for the calculation of a new attenuation map. The conversion between HU data and attenuation coefficients was performed by the PET/CT scanner software [22]. The same reconstruction protocol was used as that used for the original PET/CT data. The reconstructed PET images were then transferred to a PC for analysis.

PET/CT scans were acquired over the entire head and neck region for seven of the eight patients (excluding patient 1). The MR studies were, however, performed with a conventional head coil, which implies that the sCT images covered only the head. This required special handling during co-registration and reconstruction. We found that it was necessary to discard most of the CT slices below the head to obtain a successful co-registration of the sCT images and the CT images. We also found that we had to add the neck slices from the CT image series to the sCT image series prior to PET reconstruction. Setting the neck region to the HU value of air, because of the missing data below the head in the sCT series, underestimated the intensity of the lowest PET slices because of the 3D PET acquisition and reconstruction.

Evaluation

The PET images reconstructed with the sCT-based attenuation map (hereafter called PET_{sCTAC}) were compared to the original PET images reconstructed with the CT-based attenuation map (hereafter called PET_{CTAC}) in order to evaluate difference in the attenuation correction. The same procedure was performed with the PET images reconstructed with the sCT-based attenuation map without bone (hereafter called PET_{ACsoft}). For patients 2–8, the PET slices from the top of the skull, down to about 1 cm below the lowest part of the cerebellum were included in the evaluation. The average number of PET slices included was 52, from a total of 119 slices over the head and neck region. For patient 1, only 47 slices were available since the images had been acquired from a single bed position. In this case the entire dynamic image series was summed to give one average image volume for the evaluation.

In quantitative imaging, error estimations in all voxels should ideally be presented based on the actual uptake distribution. To support such calculations, the reconstructed images were evaluated by calculating the relative differences in all voxels in the previously described slices of the head that were included. The relative differences in percent (RD) were calculated voxel-wise:

$$\mathrm{RD} = 100\frac{(\mathrm{PET}_{\mathrm{sCTAC}} - \mathrm{PET}_{\mathrm{CTAC}})}{\mathrm{PET}_{\mathrm{CTAC}}} \quad (2)$$

This calculation was then repeated for the PET_{ACsoft} images. Since the PET images included voxels of value 0 and background counts in air outside the head, it was necessary to set a lower limit of voxel values to be included in the analysis. We found that a limit of 1 % of the highest uptake value in the head in the PET_{CTAC} images was sufficient to remove the background in air from the analysis, and therefore this limit was chosen. RD images of the whole

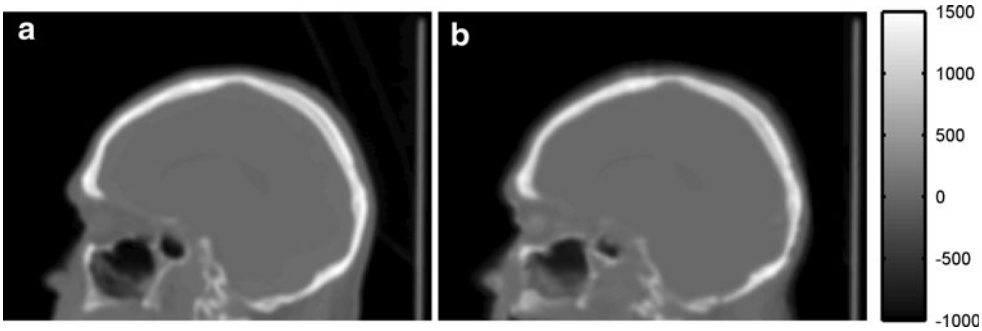

Fig. 1 CT image (**a**) and the aligned sCT image (**b**) for patient 6, scan 1. The scaling on the *colour bar* is in HU

head were then calculated for each study, as well as histograms of the RD values included in the analysis. The average RD values, standard deviations of the RD and the maximum and minimum RD values were calculated from the histograms.

The brain is particularly interesting when evaluating uptake in the head, and we carried out a separate evaluation of brain uptake. Segmentation of the brain was necessary for this analysis, but the low ^{18}F-FLT uptake in the brain makes it very difficult to use PET images for segmentation. It was however found that the image determined from the first echo of the 10° flip angle UTE sequence could be used. Using SPM8, the brain was segmented into two masks representing grey and white matter, and the two masks were added to give a single brain mask. For patient 2, some cerebrospinal fluid outside the brain was included in the brain mask, probably due to small movement artefacts in the UTE images. The cerebrospinal fluid was removed with a morphological erosion operation that was repeated three times. It should be noted that the tumour region was not segmented as brain tissue, and was not included in the brain mask, for all patients. The brain mask was then co-registered to the patient's CT image volume, as described previously for the sCT images, and was recalculated to the PET image FOV and voxel resolution using imlook4d. The voxel values within the mask were then rounded to either 0 or 1, and the resulting mask was multiplied by the PET image volumes. RD values were then calculated, and no lower limit was needed in this case since the brain contained no voxel values of 0. As for the head analysis, RD images, histograms, average values, standard deviations and maximum and minimum values were determined.

The primary interest of the ^{18}F-FLT PET images is, of course, the tumour, and a separate analysis of tumour uptake was therefore performed. For each patient scan, a volume of interest (VOI) was defined around the tumour contours in the PET_{CTAC} images using imlook4d. Two of the authors, AL (medical physicist) and TA (radiation oncologist), were involved in defining the tumour VOIs. First, an irregularly shaped region of interest (ROI), covering the tumour with some margin, was drawn manually around the tumour contours in the transaxial image showing the central slice of the tumour. This ROI was then copied to all transaxial slices above and below where that tumour was seen on the PET image, thus, resulting in a VOI. This large VOI was then shrunk to define the tumour contours by using a threshold, within the VOI, for the tumour uptake. The threshold (T) was calculated as:

$$T = B + 2\sigma_B \quad (3)$$

where B is the background surrounding the tumour, and σ_B is the background standard deviation. The background and its standard deviation were determined from a ROI contralateral to the tumour in the image showing the central slice of the tumour. The threshold method was not perfect, and for most of the patients, small background spots above the threshold, outside of the tumour, had to be manually removed to not be included in the tumour VOI. The tumour VOI was then copied to the corresponding PET_{sCTAC} and PET_{ACsoft} images, and the average value in each VOI was recorded and saved. The ratios of the PET_{sCTAC} and the PET_{ACsoft} VOI values to the PET_{CTAC} VOI value were then calculated.

Results

Table 1 presents results for the 16 PET_{sCTAC} reconstructions. The sCT method for attenuation correction gives fairly stable results across all patients. The average RD values for both the head and brain analysis show that the differences compared to PET_{CTAC} images are all less than 3.3 %. The highest average difference between scan session 1 and session 2 for an individual patient is 0.8 %. Table 1 shows that the sCT method slightly underestimates the average uptake, by about 1.6 % in the head and 1.9 % in the brain. Tumour VOI measurements are also underestimated by about the same amount: 1.5 % on average.

Table 1 shows that the standard deviations of RD in the head are relatively high, 13.2 % on average. Figure 2 presents an RD image of the head (patient 6, scan 1), where the sagittal image shows the same slice of the head as the CT and sCT images presented in Fig. 1. The differences in HU values in the nasal septa regions which are clearly visible in Fig. 1, result in the large RD values presented in Fig. 2. Table 1 shows that the RD values within the head have a relatively wide range, −90 to +283 %, and we have seen that the extreme values are found in the nasal septa region. The histogram in Fig. 2, however, makes it clear that the extreme values are rare, and are located in single voxels. The standard deviations for the brain analysis are considerably lower, 4.1 % on average. Figure 3 shows an RD image of the brain for patient 6, where it can be seen that the problems in the nasal region affect also the lowest part of the brain. The ranges of RD values are lower, −61 to +34 %, and the extreme values are located at interfaces in the cerebellum.

Table 2 presents results for the 16 PET_{ACsoft} reconstructions, which excluded bone. In this case, the values for the head are underestimated by about 11 %, and those for the brain by about 6.5 %, when compared to the PET_{CTAC} images. The tumour uptakes show the same pattern, as can be seen from the VOI measurements. Figure 4 presents an RD image of the head for patient 6 with the same slicing as in Fig. 2. The differences are higher in bone tissue and regions close to bone than they are in Fig. 2. Figure 5 shows the corresponding RD image of the brain, where

Table 1 Results from the comparison of PET_{sCTAC} and PET_{CTAC} images

	Scan no.	Head mean RD	Head std (RD)	Head RD range	Brain mean RD	Brain std (RD)	Brain RD range	Tumour ratio
Pat 1	1	−3.2	10.9	−93 to 235	−2.2	4.2	−57 to 26	0.977
	2	−2.4	11.0	−93 to 440	−2.1	4.2	−51 to 31	0.982
Pat 2	1	−0.6	15.0	−93 to 252	−2.2	4.2	−44 to 30	0.996
	2	−0.3	15.4	−91 to 320	−2.3	4.4	−48 to 28	0.998
Pat 3	1	−2.2	14.3	−78 to 311	−1.2	3.5	−60 to 41	0.958
	2	−2.9	15.1	−82 to 271	−1.9	3.7	−59 to 61	0.956
Pat 4	1	−1.8	12.0	−91 to 196	−1.7	4.5	−59 to 34	1.002
	2	−1.5	13.7	−92 to 342	−1.6	4.4	−61 to 34	1.012
Pat 5	1	−1.6	10.4	−87 to 140	−1.6	3.8	−63 to 26	0.981
	2	−1.4	13.7	−89 to 412	−1.8	4.2	−68 to 44	0.982
Pat 6	1	−1.0	15.8	−93 to 347	−1.7	4.2	−77 to 55	0.992
	2	−1.3	13.9	−96 to 282	−1.7	4.1	−85 to 39	0.993
Pat 7	1	−1.0	10.3	−85 to 170	−2.2	4.0	−42 to 21	0.975
	2	−0.6	11.3	−81 to 183	−1.9	3.9	−39 to 23	0.976
Pat 8	1	−1.7	14.7	−100 to 314	−2.3	3.9	−82 to 32	0.988
	2	−2.3	14.3	−91 to 310	−2.0	4.0	−86 to 24	0.996
Mean		−1.6	13.2	−90 to 283	−1.9	4.1	−61 to 34	0.985

Relative differences (RD) are given in percent, and "std" denotes the standard deviation. The tumour ratio is the average value in the PET_{sCTAC} tumour VOI divided by the average value in the PET_{CTAC} VOI

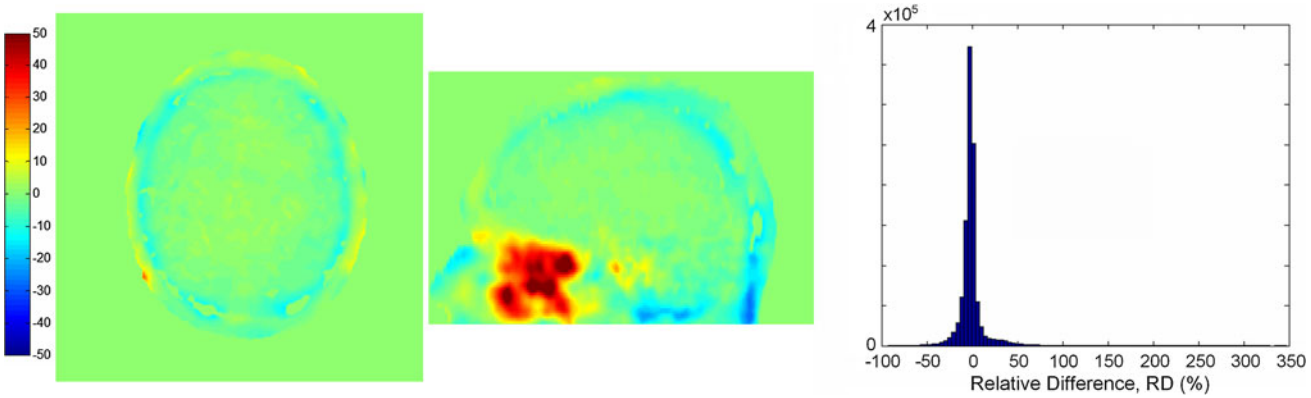

Fig. 2 RD image of the head for patient 6, scan 1, for the PET_{sCTAC} images. The scaling on the *colour bar* is in percent. The empty spots in the skull bone were not included in the analysis because of low PET uptake (less than 1 % of maximum value)

negative deviations in the part of the cortex closest to the skull bone are apparent.

Discussion

In this study, sCT images derived from a set of MR sequences have been evaluated for the purpose of attenuation correction of PET/MR imaging of the head. Images from a project evaluating early treatment response of high-grade glioma tumours were used, and results for the head, brain and tumour were analysed. The tumour uptake was only underestimated by 1.5 % on average when using the sCT method for attenuation correction. All tumours in this study were located in the cerebrum, which is the typical localisation for high-grade gliomas. The tumours with the highest negative deviations (for Patients 1, 3 and 7) were located relatively high above the orbitomeatal plane, where the PET_{sCTAC} images are underestimated, as Fig. 3 shows. The only case with an overestimated tumour uptake was for patient 4, who had a tumour located in a central section of the brain. Figure 6 shows an example of a tumour image (patient 2, scan 1). The PET tumour uptake is displayed as a fusion on two different window settings of the sCT image, and on a T1-weighted MR image. The high uptake in tumour tissue is clearly visible, and can be related both

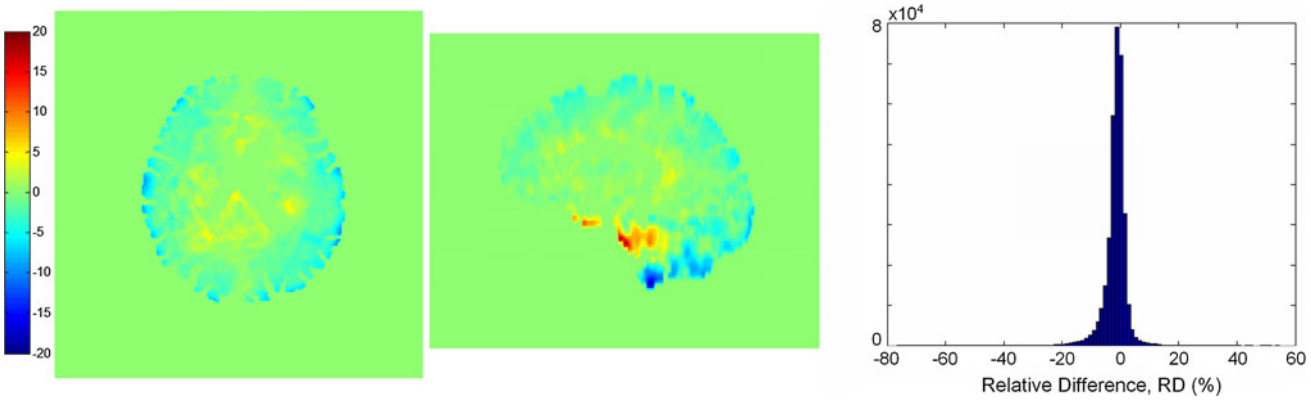

Fig. 3 RD image of the brain for patient 6, scan 1, for the PET_{sCTAC} images. The scaling on the *colour bar* is in percent (note the difference in scaling from Fig. 2)

Table 2 Results from the comparison of PET_{ACsoft} and PET_{CTAC} images

	Scan no	Head mean RD	Head std (RD)	Head RD range	Brain mean RD	Brain std (RD)	Brain RD range	Tumour ratio
Pat 1	1	−13.2	16.9	−95 to 232	−5.7	9.79	−73 to 32	0.912
	2	−12.2	16.8	−95 to 424	−5.5	9.68	−72 to 43	0.918
Pat 2	1	−8.8	19.0	−93 to 247	−9.4	11.20	−76 to 22	0.944
	2	−8.7	19.6	−92 to 319	−9.9	11.76	−83 to 22	0.949
Pat 3	1	−8.6	17.1	−85 to 274	−4.0	5.95	−67 to 42	0.923
	2	−9.4	17.5	−87 to 261	−5.2	5.89	−68 to 43	0.916
Pat 4	1	−10.0	17.5	−93 to 183	−4.6	11.4	−77 to 38	0.910
	2	−10.3	18.5	−92 to 308	−6.4	10.1	−72 to 35	0.916
Pat 5	1	−10.5	17.3	−89 to 172	−6.5	7.8	−69 to 28	0.912
	2	−9.9	19.0	−89 to 400	−6.6	8.2	−81 to 29	0.907
Pat 6	1	−11.8	22.1	−95 to 321	−6.6	9.0	−88 to 59	0.935
	2	−11.5	19.5	−96 to 272	−7.0	8.4	−88 to 34	0.935
Pat 7	1	−10.1	17.1	−89 to 152	−5.8	7.8	−69 to 28	0.889
	2	−9.2	17.0	−90 to 169	−5.6	7.5	−60 to 36	0.888
Pat 8	1	−13.4	21.5	−100 to 314	−7.4	10.6	−89 to 38	0.905
	2	−13.8	21.0	−98 to 301	−7.9	10.6	−90 to 48	0.907
Mean		−10.7	18.6	−92 to 272	−6.5	9.1	−76 to 36	0.917

Relative differences (RD) are given in percent, and "std" denotes the standard deviation. The tumour ratio is the average value in the PET_{ACsoft} tumour VOI divided by the average value in the PET_{CTAC} VOI

to the high electron density of bone visualised in the sCT images, and to the high soft-tissue contrast of MRI, using the sCT method in a PET/MR acquisition.

The results show that the major challenge for the method is the nasal septa region. The sCT images are most dissimilar from CT images at interfaces between air and tissue, where the MR images suffer from magnetic susceptibility effects and partial volume effects [16]. Relatively large differences in PET uptake can also be seen around the auditory meatuses. High-precision PET quantification in these regions is therefore not possible using the proposed method for MR-based attenuation correction.

Figure 2 shows that the RD images deviated somewhat in high-density bone regions. The deviations are due to a bias in the sCT model, caused by insufficient discrimination between dense bone and air–tissue interfaces [15]. Some small spots, for example around the outer parts of the ear, are also present in the difference images, and are most likely due to co-registration errors. Fixation and positioning of the patient differs between the PET/CT and the MR scanner, and errors in non-rigid parts of the head are to be expected. These errors do not, of course, affect the performance of the method, but contribute to the standard deviations in Tables 1 and 2. It should also be mentioned that approximately 2 weeks passed between the sCT scan and the second PET/CT scan. No major structural differences occurred during this period, but we could see minor differences in soft tissue swelling between the two

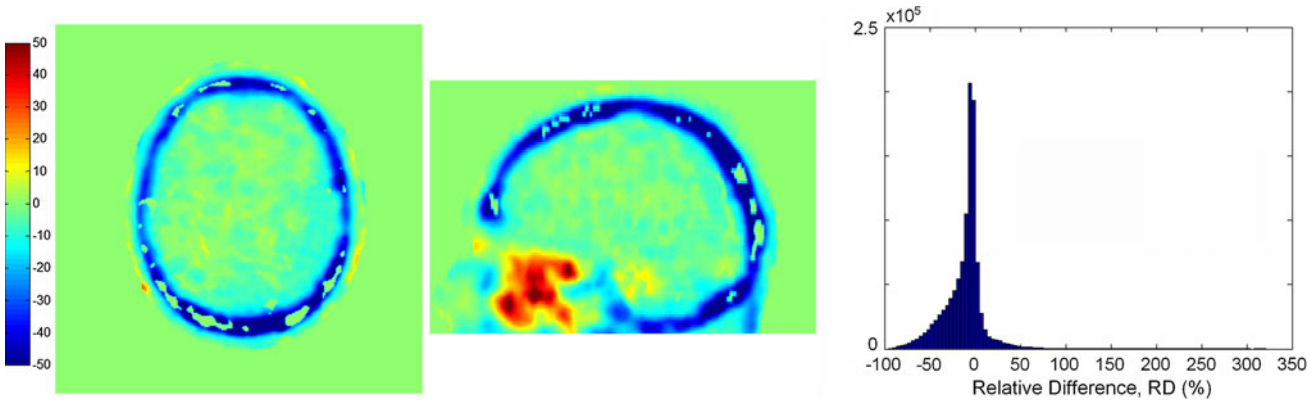

Fig. 4 RD image of the head for patient 6, scan 1, for the PET_{ACsoft} images. The scaling on the *colour bar* is in percent. The empty spots in the skull bone were not included in the analysis because of low PET uptake (less than 1 % of maximum value)

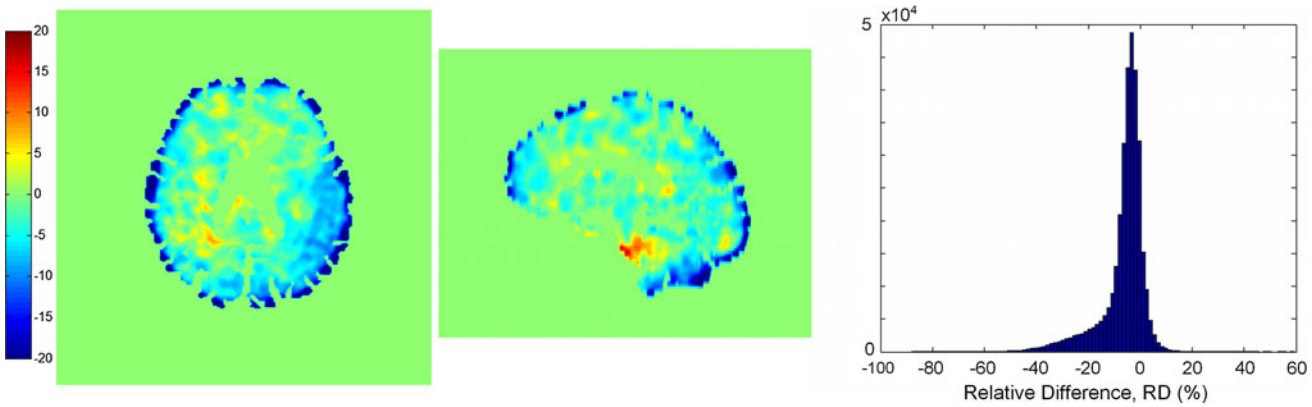

Fig. 5 RD image of the brain for patient 6, scan 1, for the PET_{ACsoft} images. The scaling on the *colour bar* is in percent (note the difference in scaling from Fig. 4)

examinations. This, together with co-registration uncertainties, contributes to the standard deviations and the differences in results between session 1 and 2 for each patient.

PET_{sCTAC} data from the separate analysis of the brain corresponds fairly well to the PET_{CTAC} data. The average RD in brain tissue is only −1.9 %, ranging from −61 to +34 %, and the histograms show that the extreme values were rare. These are mostly located at interfaces in the cerebellum. The standard deviations of the RD values within the brain are of the order of 4 % for all patients, and this value includes the relatively large differences in the cerebellum. It is difficult to compare results between studies, but within the brain, our results seem as reliable or more reliable than those obtained with methods that use UTE sequences as a basis for segmentation into different tissue classes. Keereman et al. [5] reported an average difference of 5 %. The difference images we have produced seem to be better than those of Keereman et al., in which differences of the order of −50 % were present close to the skull bone. Our maximum and minimum RD values are, however, generally somewhat higher. This may be a consequence of the high spatial resolution of the PET images in this study, using SharpIR and a Gaussian filter of only 3 mm FWHM. Smoother PET images would probably have smoothed out some of the extreme values. The difference images presented by Catana et al. [9] are similar to those presented by us, and deviations of around 20 % are present in the difficult regions in the lower part of the brain. Other results are difficult to compare. Our results from the brain lead us to believe that it is possible to apply our method in other types of brain PET/MR studies, such as PET/MR dementia imaging with ^{18}F-FDG. Semi-quantitative methods in which the cerebellum is used as a reference region should, however, be avoided. The general pattern of regions with overestimation or underestimation of activity, of around 5 % as demonstrated in Fig. 3, must also be considered when applying the method.

As can be seen in Table 1, the average PET_{sCTAC} results are underestimated up to 1.9 %. Part of the cause of the general underestimation may be that some supporting material visible in the CT images could not be added to the

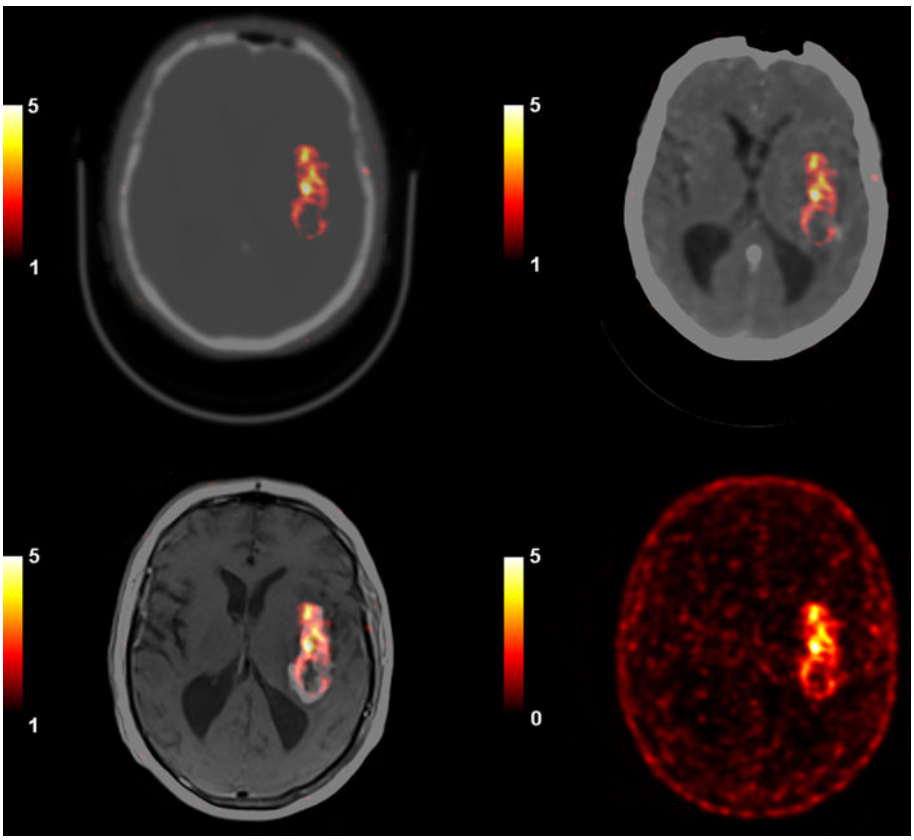

Fig. 6 ^{18}F-FLT image of high-grade malignant glioma (patient 2, scan 1), displayed in standardised uptake value (SUV) scaling. The PET image (*lower right*) is fused onto a sCT image with a bone window (*upper left*) and the same sCT image with a brain window (*upper right*). A fusion with a T1-weighted MR image is also presented (*lower left*). The sCT image used for fusion has been smoothed with a 3 mm Gaussian filter kernel to be used for attenuation correction

corresponding sCT images. A small gap between the patient and the supporting material in the head holder was necessary when drawing the head holder ROI, since the same ROI was applied to all CT images, and the body contour varied between slices. A failure to include all supporting material in attenuation correction can cause errors of up to 8 % [23].

The evaluation presented here is somewhat unconventional since the PET study was performed using ^{18}F-FLT, instead of the more commonly used ^{18}F-FDG. Relatively high activities were located in the superficial parts of the head, such as skin and blood background, which makes the comparison sensitive to co-registration errors. FLT uptake in normal brain is lower than that of FDG, in a range of 250–500 Bq/cm^3 for patients 2–8 in this study according to a ROI analysis, and this also may have introduced uncertainty into the brain evaluation. Using ^{18}F-FDG would also have made it possible to compute a brain mask directly from the PET images, thereby limiting the error propagation from image misalignments.

In contrast, adding the CT slices below the head to the sCT image series may have biased the results in the positive direction. These slices contribute to the attenuation correction in the lowest part of the head to a small degree, due to the 3D image reconstruction. Ideally, the PET/CT and MRI examinations should have covered exactly the same section of the head, but that was not possible due to consideration of factors relating to the main project.

The comparison with the attenuation correction excluding bone suggests that including bone in the sCT method is advantageous when the method is used for attenuation correction. The average tumour uptake was 8.3 % too low when bone was replaced by soft tissue. These results agree with those of Catana et al. [9], showing that intensities in the brain are underestimated when bone is excluded.

The results presented here are based on images from a 1.5 T MR scanner, whereas commercial PET/MR systems are based on 3 T scanners. The sCT method can be implemented on a 3 T scanner. Some sequence optimisation would, however, be required, as would construction of a new GMR model. It would also be interesting to apply the sCT method to images from other parts of the body. This requires shorter MR acquisition times, and new GMR models that include other tissues.

Conclusion

The sCT method for attenuation correction can be used to estimate tumour uptake, and it should be possible to use the method for hybrid PET/MR images of the brain. Further

work is required to develop the method such that it provides high accuracy in all anatomical regions of the head. Using the sCT method in hybrid PET/MR images also makes it possible to fuse PET images onto CT-like images, thereby relating PET uptake to bone structures.

Acknowledgments We would like to thank Siemens Healthcare for providing their UTE sequence for this study. This study was jointly supported by the Faculty of Medicine at Umeå University, the University Hospital of Umeå, the Centre for Biomedical Engineering and Physics at Umeå University (CMTF) through EU-project Objective 2 funding, and the Cancer Research Foundation in Northern Sweden.

References

1. von Schulthess G, Schlemmer H (2009) A look ahead: PET/MR versus PET/CT. Eur J Nucl Med Mol Imaging 36(Suppl 1):S3–S9
2. Herzog H, Van Den Hoff J (2012) Combined PET/MR systems: an overview and comparison of currently available options. Q J Nucl Med Mol Imaging 56(3):247–267
3. Kinahan PE, Townsend DW, Beyer T, Sashin D (1998) Attenuation correction for a combined 3D PET/CT scanner. Med Phys 25:2046–2053
4. Hofmann M, Pichler B, Schölkopf B, Beyer T (2009) Towards quantitative PET/MRI: a review of MR-based attenuation correction techniques. Eur J Nucl Med Mol Imaging 36(Suppl 1):S93–S104
5. Keereman V, Fierens Y, Broux T, De Deene Y, Lonneux M, Vandenberghe S (2010) MRI-based attenuation correction for PET/MRI using ultrashort echo time sequences. J Nucl Med 51:812–818
6. Salomon A, Goedicke A, Schweizer B, Aach T, Schulz V (2011) Simultaneous reconstruction of activity and attenuation for PET/MR. IEEE Trans Med Imaging 30(3):804–813
7. Martinez-Möller A, Souvatzoglou M, Delso G, Bundschuh RA, Chefd'hotel C, Ziegler SI, Navab N, Schwaiger M, Nekolla SG (2009) Tissue classification as a potential approach for attenuation correction in whole-body PET/MRI: evaluation with PET/CT data. J Nucl Med 50:520–526
8. Le Goff-Rougetet R, Frouin V, Mangin J-F, Bendriem B (1994) Segmented MR images for brain attenuation correction in PET. In: Proceedings of SPIE medical imaging: image processing, Newport Beach, California, p 725
9. Catana C, van der Kouwe A, Benner T, Michel CJ, Hamm M, Fenchel M, Fischl B, Rosen B, Schmand M, Sorensen AG (2010) Toward implementing an MRI-based PET attenuation-correction method for neurologic studies on the MR-PET brain prototype. J Nucl Med 51:1431–1438
10. Hofmann M, Bezrukov I, Mantlik F, Aschoff P, Steinke F, Beyer T, Pichler BJ, Schölkopf B (2011) MRI-based attenuation correction for whole-body PET/MRI: quantitative evaluation of segmentation- and atlas-based methods. J Nucl Med 52(9): 1392–1399
11. Malone IB, Ansorge RE, Williams GB, Nestor PJ, Carpenter TA, Fryer TD (2011) Attenuation correction methods suitable for brain imaging with a PET/MRI scanner: a comparison of tissue atlas and template attenuation map approaches. J Nucl Med 52(7):1142–1149
12. Schulz V, Torres-Espallardo I, Renisch S, Hu Z, Ojha N, Börnert P, Perkuhn M, Niendorf T, Schäfer WM, Brockmann H, Krohn T, Buhl A, Günther RW, Mottaghy FM, Krombach GA (2011) Automatic, three-segment, MR-based attenuation correction for whole-body PET/MR data. Eur J Nucl Med Mol Imaging 38(1):138–152
13. Wagenknecht G, Kops ER, Mantlik F, Fried E, Pilz T, Hautzel H, Tellmann L, Pichler BJ, Herzog H (2011) Attenuation correction in MR-BrainPET with segmented T1-weighted MR images of the patient's head — A comparative study with CT. In: Proceedings of the IEEE NSS/MIC conference, Valencia, p 2261
14. Robson M, Gatehouse P, Bydder M, Bydder G (2003) Magnetic resonance: an introduction to ultrashort TE (UTE) imaging. J Comput Assist Tomogr 27:825–846
15. Johansson A, Karlsson M, Nyholm T (2011) CT substitute derived from MRI sequences with ultrashort echo time. Med Phys 38(5):2708–2714
16. Johansson A, Karlsson M, Yu J, Asklund T, Nyholm T (2012) Voxel-wise uncertainty in CT substitute derived from MRI. Med Phys 39(6):3283–3290
17. Stupp R, Mason WP, van den Bent MJ, Weller M, Fisher B, Taphoorn MJ, Belanger K et al (2005) Radiotherapy plus concomitant and adjuvant temozolomide for glioblastoma. N Engl J Med 352(10):987–996
18. Shields A, Grierson J, Dohmen BM, Machulla HJ, Stayanoff JC, Lawhorn-Crews JM, Obradovich JE, Muzik O, Mangner TJ (1998) Imaging proliferation in vivo with F-18 FLT and positron emission tomography. Nat Med 4:1334–1336
19. Chen W, Cloughesy T, Kamdar N, Satyamurthy N, Bergsneider M, Liau L, Mischel P, Czernin J, Phelps ME, Silverman DHS (2005) Imaging proliferation in brain tumors with 18F-FLT PET: comparison with 18F-FDG. J Nucl Med 46:945–952
20. Doran S, Charles-Edwards L, Reinsberg S, Leach M (2005) A complete distortion correction for MR images: I. Gradient warp correction. Phys Med Biol 50:1343–1361
21. Valentin J (ed) (2003) ICRP Publication 89. Basic anatomical and physiological data for use in radiological protection: reference values. Elsevier Science Ltd, Oxford
22. Burger C, Goerres G, Schoenes S, Buck A, Lonn AH, Von Schulthess GK (2002) PET attenuation coefficients from CT images: experimental evaluation of the transformation of CT into PET 511-keV attenuation coefficients. Eur J Nucl Med Mol Imaging 29:922–927
23. Mantlik F, Hofmann M, Werner MK, Sauter A, Kupferschläger J, Schölkopf BJ, Pichler B, Beyer T (2011) The effect of patient positioning aids on PET quantification in PET/MR imaging. Eur J Nucl Med Mol Imaging 38:920–929